# Benchmark of Electromagnetic Gyrokinetic Codes in High Performance Fusion Plasma[*)]

Shinya MAEYAMA, Tomo-Hiko WATANABE, Hauke DOERK[1)], Motoki NAKATA[2)] and
Akihiro ISHIZAWA[3)]

*Nagoya University, Furo-cho, Nagoya 464-8602, Japan*
[1)]*Max-Planck-Institut für Plasmaphysik, Boltzmannstraße 2, D-85748 Garching, Germany*
[2)]*National Institute for Fusion Science, 322-6 Toki, Gifu 509-5292, Japan*
[3)]*Kyoto University, Gokasho, Uji, Kyoto 611-0011, Japan*

Benchmark between electromagnetic gyrokinetic codes GKV and GENE based on the flux tube model has been carried out by employing the high performance tokamak experiment data. The constructed flux coordinates, linear dispersion relation, and nonlinear turbulent transport show good agreements. Utilizing these codes, linear mode structures of micro-tearing modes have been examined. It is found that the current density is highly localized in the radial direction and peaks on the inner board side of the torus, while the broaden O-shape structure is observed on the torus outer board side. This broadening originates from the magnetic drift, that is, the finite orbit width of passing particles.

## 1. Introduction

In high performance fusion plasma characterized by high $\beta = \mu_0 n_0 T_0 / B_0^2$ values, micro-instabilities and associated turbulence have electromagnetic properties: stabilization of ion temperature gradient modes (ITGs), and destabilization of kinetic ballooning modes and micro-tearing modes (MTMs) [1, 2]. Although their physics is often analyzed by the gyrokinetic theory and simulations in a simplified magnetic geometry, quantitative evaluations of linear instabilities and of turbulent transport relevant to experiments require the detailed informations of the magnetic configuration, a realistic multi-species collision operator. For this purpose, a verification study based on a code-code benchmark is helpful. In this paper, we carry out linear and nonlinear benchmark tests of the electromagnetic gyrokinetic code GKV [3] against GENE [4], using data based on an ASDEX Upgrade H-mode discharge [5].

## 2. The GKV and GENE code

GKV was originally developed for the analysis of phase-space turbulence and the turbulent transport in tokamak and helical systems [3], and has recently been extended for implementing electromagnetic fluctuations, MHD equilibrium interface, and multi-species collision operator [6–11]. GENE has been developed and applied for the analysis of the electromagnetic turbulence over a

decade [4], which includes advanced physical models such as magnetic fluctuations parallel to the confinement field $\tilde{B}_\parallel$, equilibrium sheared flows, and a global model [12]. In this benchmark, both codes solve the $\delta f$ gyrokinetic Vlasov-Poisson-Ampère equations,

$$
\frac{\partial \tilde{f}_s}{\partial t} + \left( v_\parallel \nabla_\parallel + \boldsymbol{v}_{\mathrm{ds}} \cdot \nabla_\perp - \frac{\mu \nabla_\parallel B}{m_s} \right) \tilde{f}_s
$$
$$
= -\frac{e_s F_{\mathrm{Ms}}}{T_s} \left[ v_\parallel \left( \nabla_\parallel J_{0s}\tilde{\phi} + \frac{\partial J_{0s}\tilde{A}_\parallel}{\partial t} \right) + \boldsymbol{v}_{\mathrm{ds}} \cdot \nabla J_{0s}\tilde{\phi} \right.
$$
$$
\left. - \boldsymbol{v}_{*s} \cdot \nabla J_{0s}(\tilde{\phi} - v_\parallel \tilde{A}_\parallel) \right] + \mathcal{N}_s + C_s, \tag{1}
$$

$$
\sum_s \frac{e_s^2 n_s}{T_s} (1 - \Gamma_{0s}) \tilde{\phi} = \sum_s e_s \int dv^3 J_{0s}\tilde{f}_s, \tag{2}
$$

$$
\nabla_\perp^2 \tilde{A}_\parallel = -\mu_0 \sum_s e_s \int dv^3 J_{0s} v_\parallel \tilde{f}_s, \tag{3}
$$

where the gyrophase-average operators $J_{0s} = \oint (d\xi/2\pi) e^{\rho_s \cdot \nabla}$ and $\Gamma_{0s} = \int dv^3 (F_{\mathrm{Ms}}/n_s) J_{0s}^2$ are used with the gyroradius vector $\rho_s = \boldsymbol{b} \times m_s \boldsymbol{v}/(e_s B)$. The magnetic and diamagnetic drift velocities are given by $\boldsymbol{v}_{\mathrm{ds}} = \boldsymbol{b} \times (\mu \nabla B + m_s v_\parallel^2 \boldsymbol{b} \cdot \nabla \boldsymbol{b})/(e_s B)$ and $\boldsymbol{v}_{*s} = \boldsymbol{b} \times [T_s \nabla \ln n_s + (m_s v_\parallel^2/2 + \mu B - 3T_s/2)\nabla \ln T_s]/(e_s B)$. $\mathcal{N}_s = \boldsymbol{b} \times \nabla_\perp J_{0s}(\tilde{\phi} - v_\parallel \tilde{A}_\parallel) \cdot \nabla_\perp (\tilde{f}_s + e_s F_{\mathrm{Ms}} J_{0s}\tilde{\phi}/T_s)/B$ represents $\boldsymbol{E} \times \boldsymbol{B}$ and magnetic flutter nonlinearity, and $C_s$ is the collision operator. We employ the conventional local flux-tube model [13], with the flux coordinates $x = a(\rho - \rho_0)$, $y = (a\rho_0/q_0)[q(\rho)\theta - \zeta]$, $z = \theta$ (where the radial coordinate $\rho$ with the plasma minor radius $a$,
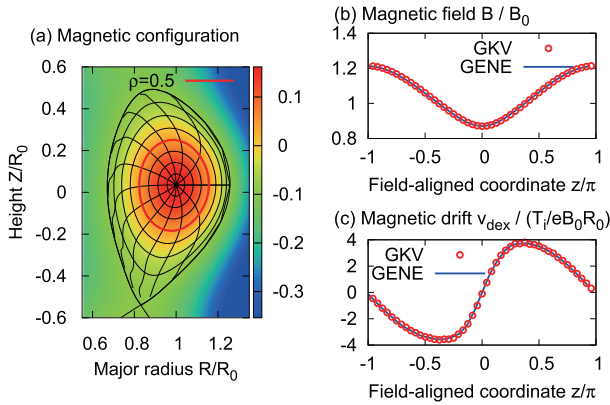
---

Fig. 1   (a) Color contour of flux function and the constructed flux coordinates on a poloidal cross section. Field-aligned profiles of (b) the magnetic field strength $B$ and of (c) the radial component of the electron magnetic drift velocity $v_{dex}$ calculated from the metrics (where $v_\parallel = 1.97 v_{te}$ and $\mu = 0.53 T_e/B_0$) at $\rho = 0.5$.

poloidal and toroidal angles $\theta$, $\zeta$), the parallel velocity $v_\parallel$ and the magnetic moment $\mu$ as velocity-space coordinates.

The ASDEX Upgrade H-mode discharge data (AUG#29224 at $\rho = 0.5$ corresponding to the case B in Ref. [5]) is used for the benchmark, which demands the electromagnetic physics, experimental equilibrium interface and multiple-species collision operator. We here neglect $\tilde{B}_\parallel$ and equilibrium sheared flows, and approximate $\boldsymbol{b} \cdot \nabla \boldsymbol{b} \simeq \nabla \ln B$ in the low-$\beta$ limit.

# 3. Benchmark Results

## 3.1   Constructed flux coordinates

Accuracy of local flux tube simulations may depend on the accuracy of the employed flux coordinates. To construct flux coordinates from the MHD equilibrium data (EQDSK format), GKV uses the interface code IGS [9], which provides Hamada, Boozer, or Axisymmetric type flux coordinates. In this benchmark the axisymmetric coordinates are employed, since it coincides with the coordinates employed in GENE (via the TRACER interface [14]). Figure 1 shows the flux coordinates constructed from the AUG#29224 data. The magnetic field and metric data calculated in GKV and GENE agree well.

It is known that, for the up-down symmetric configuration (symmetric $B, \partial_x B, \partial_y B, g^{xx}, g^{yy}, g^{yz}, g^{zz}, \sqrt{g}$, and anti-symmetric $\partial_z B, g^{xy}, g^{xz}$ for $z \to -z$), the linearized gyrokinetic equation is invariant under the parity transformation $(x, z, v_\parallel) \to (-x, -z, -v_\parallel)$ [15], which ensures the decomposition of the linear modes into the ballooning (even) parity mode $\tilde{f}_s(-x, y, -z, -v_\parallel, \mu) = \tilde{f}_s(x, y, z, v_\parallel, \mu)$, such as ITGs, and the tearing (odd) parity mode $\tilde{f}_s(-x, y, -z, -v_\parallel, \mu) = -\tilde{f}_s(x, y, z, v_\parallel, \mu)$, such as MTMs. Generally speaking the single-null configuration violates this parity symmetry. However, since the up-down asymmetric component of the equilibrium at $\rho = 0.5$ is quite
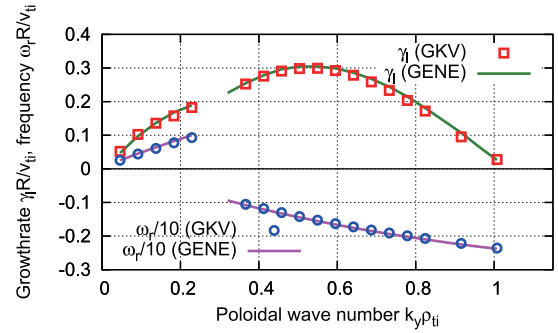


Fig. 2   Linear dispersion of MTM and ITG.

small as seen in Fig. 1, the linear modes observed in this benchmark case can be classified in either parity structure.
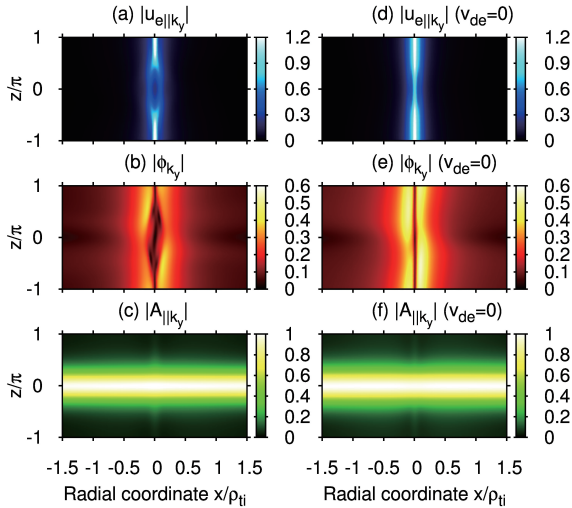
## 3.2   Linear dispersion

Employing the constructed flux coordinates, the linear dispersion relation of micro-instabilities is examined. Choosing $k_x = 0$, the ballooning space $-23\pi \le z \le 23\pi$ and velocity space $-4 \le v_\parallel/v_{te} \le 4$, $0 \le \mu B_0/T_s \le 8$ are resolved by $552 \times 64 \times 32$ grid points. Figure 2 shows good agreements between the results of GKV and GENE. From the difinition in GKV, the positive and negative frequency waves propagate in the electron and ion diamagnetic drift directions, respectively. Lower wave number $k_y\rho_{ti} < 0.3$ modes rotating in the electron diamagnetic direction and having tearing parity structures are MTMs, and the higher wave number modes rotating in the ion diamagnetic direction and having ballooning parity structures are ITGs. We found that the simple Lenard Bernstein collision operator reduces the growth rate of MTM, and the collisionless tests show ITGs become dominant even in the low wave number regime. Thus the finite collisional drive is confirmed to be affected by the details of the collision operator. Nevertheless, Sugama's self-adjoint collision operator in GKV [16] and Landau-Boltzmann collision operator in GENE [17] here capture equivalent physics for the destabilization of MTMs.

Hereafter, we will focus on the physics of MTMs. Most of theoretical works were engaged in the sheared slab geometry [2, 18], while some literatures dealt with toroidal plasma with trapped particle effects but neglecting the magnetic drift [19]. Recent gyrokinetic simulation studies using GS2 [20], however, reported the importance of the magnetic drift for the destabilization of MTMs in spherical tokamak [21, 22]. Being stimulated by these reports, we have carried out GKV simulations, to investigate the linear properties of toroidal MTMs in ASDEX Upgrade. The results are summarized in Table 1. As expected, contribution of the perturbed ion distribution function (but the polarization is retained in Poisson equation) and up-down asymmetry of magnetic configuration are negligible. Additionally, since the mirror force term is also less effective, effect of trapped electron dissipation pointed out

Table 1  Linear growth rate $\gamma_l$ and real frequency $\omega_r$ with respect to various numerical settings (for $k_y\rho_{ti} = 0.183$ MTM).

| Numerical setting | $\gamma_l R/v_{ti}$ | $\omega_r R/v_{ti}$ |
|---|---|---|
| Default | 0.154 | 0.796 |
| $\tilde{f}_i = 0$ | 0.149 | 0.829 |
| Up-down symmetrization | 0.149 | 0.802 |
| $\mu\nabla_\parallel B/m_s = 0$ | 0.148 | 0.929 |
| $\tilde{\phi} = 0$ | 0.100 | 0.712 |
| $v_{ds} = 0$ | 0.061 | 0.799 |



(a) $|u_{e\parallel k_y}|$  (d) $|u_{e\parallel k_y}|$ ($v_{de}=0$)

(b) $|\phi_{k_y}|$  (e) $|\phi_{k_y}|$ ($v_{de}=0$)

(c) $|A_{\parallel k_y}|$  (f) $|A_{\parallel k_y}|$ ($v_{de}=0$)

Radial coordinate $x/\rho_{ti}$

Fig. 3  Electron parallel flow $|\tilde{u}_{e\parallel k_y}/(n_0 v_{te})|$, electrostatic potential $|\tilde{\phi}_{k_y}/(T_i/e)|$ and parallel vector potential $|\tilde{A}_{\parallel k_y}/(T_i/ev_A)|$ structures in radial $x$ and field-aligned $z$ coordinates, where the amplitude is normalized by $ev_A\tilde{A}_{\parallel k_y}/T_i$ at $(x,z) = (0,0)$. The left column (a) - (c) and the right column (d) - (f) correspond to the default and the no magnetic drift ($v_{ds} = 0$) cases, respectively.

in Refs. [19] is not essential here. Neglect of electrostatic potential $\phi = 0$ or of magnetic drift $v_{ds} = 0$ significantly reduce growth rate, which is similar trend with Ref. [21].

## 3.3  Linear mode structure of MTM and effects of magnetic drift

We further investigate the effect of magnetic drift on MTM. MTM has a $k_\parallel \sim 0$ resonant structure, which is represented by an extremely elongated mode structure in ballooning angle (see e.g., Ref. [21]). This elongated structure in turn creates fine radial modes in the sheared magnetic geometry [13], and the superposition of the different $k_x$ modes with the same phase forms a radially localized structure at the resonant surface.

Figure 3 shows radial $x$ and field-aligned $z$ space structure of a poloidal Fourier mode $k_y\rho_{ti} = 0.183$, where we employed high resolutions $\Delta x = 0.0132\rho_{ti}$ and $\Delta z/\pi = 0.0156$. The current structure shown in Fig. 3 (a) is highly localized in the radial direction, which peaks on the inner board side of the torus at $z = \pm\pi$. The full width at half
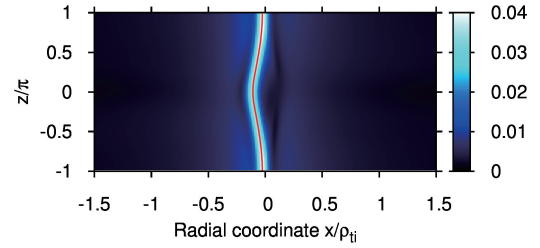


Fig. 4  Electron distribution function $|\tilde{f}_{ek_y}/(n_0 v_{te}^3)|$ in $(x,z)$ space with choosing the velocities $v_\parallel = 1.97 v_{te}$ and $\mu = 0.53 T_e/B$. For comparison, the passing particle trajectory is plotted by a solid line, which starts from the torus inner board side $z_0 = -\pi$ and $x_0 = -0.026\rho_{ti}$.

maximum of $|\tilde{u}_{e\parallel k_y}|$ at $z = -\pi$ is $\Delta_{fwhm} = 0.08\rho_{ti}$, which is almost the same as the simple slab estimate $\Delta_{fwhm}^{Est.}/\rho_{ti} = qR\omega/(\hat{s}k_y\rho_{ti}v_{te}) = 0.089$, as reported in Ref. [23]. In addition, the current structure is broaden and forms an O-shape on the torus outer board side at $z = 0$. The similar broadening at $z = 0$ is also observed in the electrostatic potential profile in Fig. 3 (b). We note that the fluctuations almost have the tearing parity: the anti-symmetric structure for $\tilde{\phi}_{k_y}(-x,-z) = -\tilde{\phi}_{k_y}(x,z)$, and the symmetric one for $\tilde{u}_{e\parallel k_y}(-x,-z) = \tilde{u}_{e\parallel k_y}(x,z)$, $\tilde{A}_{\parallel k_y}(-x,-z) = \tilde{A}_{\parallel k_y}(x,z)$. The $k_x = 0$ component is dominant in $\tilde{A}_\parallel$ which corresponds to theoretically assumed "constant $\tilde{A}_\parallel$" approximation. In the flux-tube model, the Laplacian operator is $\nabla_\perp^2 = g^{xx}\partial_x^2 + i2g^{xy}k_y\partial_x - g^{yy}k_y^2$, and the second derivative $\partial_x^2\tilde{A}_\parallel$ coincides with the localized current structure.

In contrast, the O-shape broadening at $z = 0$ has not been observed in the case of neglecting the magnetic drift $v_{ds} = 0$, which clearly shows that the magnetic drift affects the mode structure of MTM. The O-shape mode structure is associated with the particle trajectory given by parallel and magnetic drift motions, i.e., the finite orbit width of the passing particles. Neglecting the magnetic mirror force, the electron motions in the $x$ and $z$ directions is approximated by $\dot{z} = \pm v_\parallel \boldsymbol{b}\cdot\nabla z$ and $\dot{x} = \boldsymbol{v}_{de}\cdot\nabla x$. Figure 4 directly compares the calculated passing particle trajectory and the contour of electron distribution function $|\tilde{f}_{ek_y}|$ for $v_\parallel = 1.97 v_{te}$ and $\mu = 0.53 T_e/B$. The result demonstrates that the electron current density in $x < 0$ is caused by the $v_\parallel > 0$ perturbation advected from $z = -\pi$, and that the trajectory is bended by the magnetic drift. Equally, the current density in $x > 0$ is caused by the $v_\parallel < 0$ perturbation started from $z = +\pi$. It is consistent with the tearing parity, $\tilde{f}_{ek_y}(-x,-z,-v_\parallel,\mu) = -\tilde{f}_{ek_y}(x,z,v_\parallel,\mu)$ and $\tilde{u}_{e\parallel k_y}(-x,-z) = \tilde{u}_{e\parallel k_y}(x,z)$. From these trajectory analysis, perturbations of the electron distribution function seem to be driven on the torus inner board side at $z = \pm\pi$ and advected to the outer board side (if perturbations were driven on the torus outer board side, the X-point and O-point are observed at $z = 0$ and $z = \pm\pi$, respectively, in contrast to the simulation result).
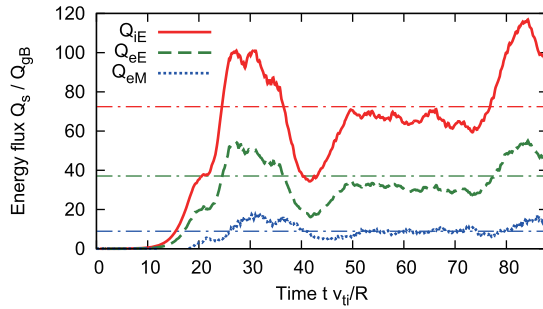
From Fig. 3 (a), we have evaluated the peak-to-peak

Fig. 5 Time evolution of energy fluxes normalized by gyro-Bohm flux $Q_{gB} = n_0 T_i v_{ti} \rho_{ti}^2 / R_0^2$. The solid, dash and dotted lines represent ion energy flux $Q_{iE}$, electron energy flux caused by $\boldsymbol{E} \times \boldsymbol{B}$ flows $Q_{eE}$ and magnetic flutter $Q_{eM}$, respectively. For references, time-averaged values obtained by GENE (from Fig. 5 in Ref. [5]) are plotted by chain lines.

width of the electron current density at $z = 0$ as $\Delta_{FOW} = 0.18\rho_{ti}$. If one approximates $\dot{z} \sim v_{\parallel}/(qR_0)$ and $\dot{x} \sim (m_e v_{\parallel}^2 + \mu B_0) \sin z/(eB_0 R_0)$, with thermal speed $v_{\parallel} = v_{te}$ and $\mu = T_e/(2B_0)$, the finite orbit width can be analytically given by $\Delta_{FOW}^{Est.}/\rho_{ti} = 4q(m_e v_{\parallel}^2 + \mu B_0)/(m_i v_{ti} v_{\parallel}) = 0.132$, which roughly agrees with the width of the O-shape structure.

### 3.4 Turbulent transport: preliminary nonlinear benchmark

We have also carried out a nonlinear simulation of MTM/ITG driven turbulence, where the domain sizes $-50.7 \leq x/\rho_{ti} \leq 50.7$, $-68.6 \leq y/\rho_{ti} \leq 68.6$, $-\pi \leq z \leq \pi$, $-4 \leq v_{\parallel}/v_{ts} \leq 4$ and $0 \leq \mu B_0/T_s \leq 8$ are resolved by $288 \times 96 \times 48 \times 96 \times 32$ grid points, respectively. Agreements of turbulent transport fluxes obtained by GKV and GENE are confirmed in Fig. 5, where the effects of $\tilde{B}_{\parallel}$ and of parallel flow shear are shown to be negligible in a GENE simulation. The successful nonlinear benchmark test provides a basis for further investigations of nonlinear physics in MTM/ITG turbulence.

## 4. Summary and Discussion

Recent extensions of GKV introducing the tokamak MHD equilibrium interface and the multi-species collision operator enable us the MTM/ITG simulations of an ASDEX Upgrade high performance discharge. We have confirmed good agreements between GKV and GENE in the constructed flux coordinates, the linear dispersion of MTM/ITG, and the nonlinear turbulent transport fluxes. These provide the basis for the investigations of comprehensive physics of electromagnetic turbulence in conditions relevant to experiments.

The linear mode structure of toroidal MTM is exam-ined in detail. We have demonstrated that the magnetic drift creates a radially broaden O-shaped current structure along a field line, and its width corresponds to the finite orbit width of passing particles. The broadning is also observed in the electrostatic potential, and modifies the parallel electric field profile, possibly affecting the instability. It may be related to the previous works where the neglect of the magnetic drift and electrostatic potential significantly stabilizes the toroidal MTM in MAST [21]. Effect of the magnetic drift in the toroidal direction $v_{dey}$ may also be important, but remains for future studies.

[1] R.D. Hazeltine, D. Dobrott and T.S. Wang, Phys. Fluids **18**, 1778 (1975).
[2] J.F. Drake and Y.C. Lee, Phys. Fluids **20**, 1341 (1977).
[3] T.-H. Watanabe and H. Sugama, Nucl. Fusion **46**, 24 (2006).
[4] F. Jenko *et al.*, Phys. Plasmas **7**, 1904 (2000).
[5] H. Doerk *et al.*, Phys. Plasmas **22**, 042503 (2015).
[6] S. Maeyama *et al.*, Comput. Phys. Commun. **184**, 2462 (2013).
[7] A. Ishizawa *et al.*, Nucl. Fusion **53**, 053007 (2013).
[8] M. Nunami, T.-H. Watanabe and H. Sugama, Plasma Fusion Res. **5**, 016 (2010).
[9] M. Nakata *et al.*, Plasma Fusion Res. **9**, 1403029 (2014).
[10] M. Nunami *et al.*, Plasma Fusion Res. **10**, 1403058 (2015).
[11] M. Nakata *et al.*, Comput. Phys. Commun. **197**, 61 (2015).
[12] T. Görler *et al.*, J. Comput. Phys. **230**, 7053 (2011).
[13] M.A. Beer *et al.*, Phys. Plasmas **2**, 2687 (1995).
[14] P. Xanthopoulos and F. Jenko, Phys. Plasmas **13**, 092301 (2006).
[15] H. Sugama *et al.*, Plasma Phys. Control. Fusion **53**, 024004 (2011).
[16] H. Sugama, T.-H. Watanabe and M. Nunami, Phys. Plasmas **16**, 112503 (2009).
[17] H. Doerk, Ph.D. Dissertation Universität Ulm, 2012.
[18] N.T. Gladd *et al.*, Phys. Fluids **23**, 1182 (1980).
[19] J.W. Connor, S.C. Cowley and R.J. Hastie, Plasma Phys. Control. Fusion **32**, 799 (1990).
[20] M. Kotschenreuther, G. Rewoldt and W.M. Tang, Comput. Phys. Commun. **88**, 128 (1995).
[21] D.J. Applegate *et al.*, Plasma Phys. Control. Fusion **49**, 1113 (2007).
[22] D. Dickinson *et al.*, Plasma Phys. Control. Fusion **55**, 074006 (2013).
[23] H. Doerk *et al.*, Phys. Plasmas **19**, 055907 (2012).